Microfluidics for the synthesis of iron oxide nanoparticles

Ali Abou-Hassan, Olivier Sandre, Valérie Cabuil

Author manuscript of chapter 9: Microfluidics for the synthesis of iron oxide nanoparticles, in *Microfluidic Devices in Nanotechnology: Applications*, C.S.S.R. Kumar, Editor 2010, John Wiley & Sons, Hoboken NJ, 323-360

Microfluidic Devices for Synthesis of Iron Oxide Nanoparticles

By *Ali Abou-Hassan*, Olivier Sandre*, and *Valérie Cabuil*

((To my family))

Contents

1. Introduction

Iron oxides are widespread in nature *[1]*and are present almost everywhere in the global system, even in Mars' soil.*[2]* They are used for various applications in industry as colored pigments, magnetic materials, ferrofluids, catalysts… There are sixteen species of iron oxides, hydroxides or oxihydroxides, which will be in this chapter collectively referred to as iron oxihydroxides (Table 1). For more details on the different iron oxihydroxides the reader can refer to the book of Cornell and Shwertmann.*[3]*

Oxide hydroxides and hydroxides	Oxides
Goethite α-FeOOH	Haematite α-Fe_2O_3
Lepidocrocite γ-FeOOH	Magnetite Fe_3O_4
Akaganéite β-FeOOH	Maghemite γ- Fe_2O_3
Schwertmannite $Fe_{16}O_{16}(OH)_y(SO_4)_z.nH_2O$	β- Fe_2O_3
δ- FeOOH	ε- Fe_2O_3
Feroxyhyte δ'- FeOOH	Wüstite FeO
High pressure FeOOH	
Ferrihydrite $Fe_5HO_8.4H_2O$	
Bernalite $Fe(OH)_3$	
$Fe(OH)_2$	

Table 1: The main iron oxides. Readapted from ref *[3]*

All the iron oxihydroxides are of great interest and have numerous applications, but our review will focus only on materials widely studied these last years, i.e. magnetic iron oxides as magnetite Fe_3O_4 and maghemite γ- Fe_2O_3 nanoparticles. These materials have wide-ranging technological applications when they are divided under the form of nanoparticles, ranging from navigation with magnetite (or Lodestone) to modern high-density magnetic recording media and readhead devices.

Magnetite Fe_3O_4 is a black, ferrimagnetic mineral containing both Fe^{II} and Fe^{III} and has an inverse spinel structure. Maghemite γ- Fe_2O_3 is a red-brown, ferrimagnetic material,

isostructural with magnetite, but with cation deficient sites. When the size of magnetite or maghemite particles is reduced below about ~ 15 nm, the particles are magnetic monodomains. It means that they have a permanent magnetic moment which intensity is proportional to their volume but which direction is submitted to spontaneous fluctuations inside the grain. This magnetic moment is due to the crystalline order, characteristic of the spinel like structure. For ultrasmall particles (diameter smaller than a few nanometers), the surface disorder lead to a very important decrease of the moment.

Thus nanometric ferro- or ferrimagnetic particles behave very differently from the corresponding bulk materials and their magnetic behaviour is called *superparamagnetism.[4]* The main characteristic of superparamagnetism is the spontaneous fluctuation of the direction of the magnetic moment in the small magnetic grain, which is due to the fact that, for very small ferromagnetic particles, the magnetic anisotropy energy (KV), responsible for keeping the magnetization oriented in what is called the easy axis of magnetization is comparable to the thermal energy (k*T*). This results in a zero magnetization in zero field if the fluctuations are averaged over a timescale larger than their typical time τ.*[5]* The fluctuation time τ generally varies over a very broad time scale, depending on the size of the particles. (Figure. 1)

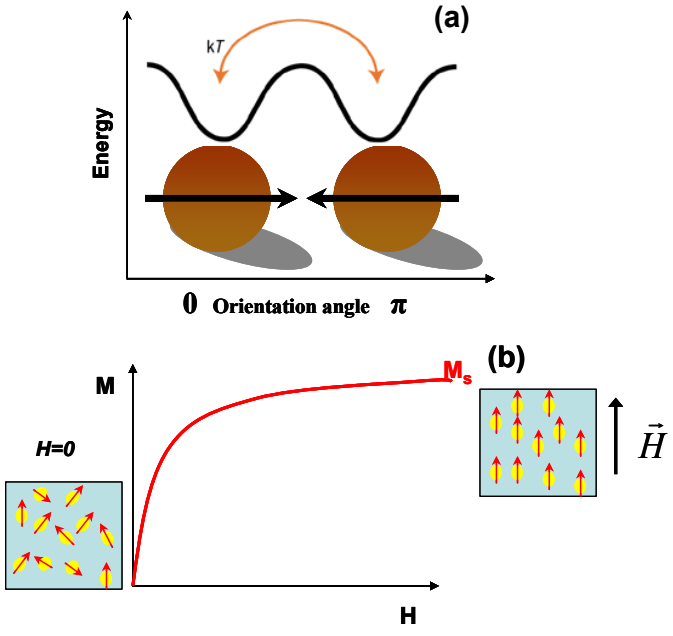

Figure 1: (a) For very small ferromagnetic (FM) particles the magnetic anisotropy energy (responsible for keeping the magnetization oriented in certain directions) is comparable to the thermal energy (kT). When this happens, the particles become superparamagnetic; as thermal fluctuations randomly flip the magnetization direction between parallel and antiparallel orientations. (b) Typical magnetization curve for superparamagnetic nanoparticles (Langevin's curve). Under a zero magnetic field, the magnetic moments are randomly oriented, but they progressively align parallel to the field direction when a magnetic field is applied. When all the magnetic

moments are aligned with the magnetic field, the curved has attained a saturation value Ms which is the product of the volume fraction Φ by the specific magnetization ms of the material (e.g. $3x10^5$ A/m for colloidal maghemite which corresponds to 33 Bohr magnetons per nm^3).

Superparamagnetism also refers to the extremely large magnetic moments that these nanoparticles bear (typically a few tens of thousand Bohr magnetons μ_B) compared to the moment of isolated ions (5.4 μ_B for Fe^{2+} and 5.9 μ_B for Fe^{3+}). When placed in external magnetic fields, the magnetization of a superparamagnetic suspension of nanoparticles is about 10^4 times larger than the magnetization a paramagnetic solution with an equivalent iron salt concentration

Ferromagnetic bulk materials, once magnetized, show remanence (i.e remain partially magnetized even in the absence of an applied field), and therefore are used as recording materials. In contrast, supeparamagnetic materials differ from ferromagnetic bulk substances, because they do not retain any magnetization once the external field is removed.*[6]*

Among others, superparamagnetic nanoparticles are largely used in magnetic storage media,*[7]* for biosensing applications,*[8]* medical applications, such as targeted drug delivery,*[9]* as contrast agents in magnetic resonance imaging,*[10]*, and as ferrofluids,*[11-14]*. For most of these applications, it is necessary to control the production of the magnetic nanoparticles, their monodispersity and their states of aggregation, as these physical parameters, control their physical and physicochemical properties.

In the past years, several research groups have proposed to use microfluidic systems as a promising strategy for obtaining high quality nanoparticles with highly monodisperse particles in a single-shot process without any subsequent size selection. The aim of this chapter is to review the recent scientific literature concerning the use of microfluidic for the synthesis of the iron oxides nanomaterials over the five last years. After a review of the main synthesis methods used to get these materials in bulk chemistry, the few works related to the synthesis of ferric oxide nanoparticles in microfluidics will be introduced.

2. Main bulk procedures for the synthesis of iron oxide nanoparticles

The Chemistry of iron oxihydroxides is very diversified and rich. Almost all the species can be formed from solutions by a polycondensation mechanism which will be the main topic of this section. For more details on the mechanisms and kinetics of the precipitation from ionic solution, the reader can refer to the ref *[15]* and ref *[16]*.

2.1 Metallic cations in solution and polycondensation.

Metal cations M^{z+} in water are solvated by dipolar water molecules giving rise to aquo-cations $[M(OH_2)_6]^{z+}$.*[17]* In the particular case of iron salts (chloride, nitrates…), dissolution in water produces hexacoordinated aquo complexes $[Fe(OH_2)_6]^{z+}$ where z = 2 or 3. The polarization of coordinated water molecules in the coordination sphere is strongly dependent on the oxidation state and size of cation. Charge transfer occurs via the Fe-OH_2 σ bond and electron density is transferred from the bonding $3a_1$ molecular orbital of coordinated water molecules towards empty orbitals of the metal cations.*[18]*

This charge transfer results into a weakening of the O-H bond within the water molecule, and the aquo complexes manifest Brønsted acid-base properties leading to the deprotonation of the coordinated water molecules:

$$[Fe(OH_2)_6]^{z+} + h\ H_2O \longrightarrow [Fe(OH)_h(OH_2)_{6-h}]^{(z-h)+} + h\ H_3O^+$$

The higher is the oxidation state of the cation, the lower is its size and the higher is the acidity of the complexe. This makes the ferric aquo complexes more acidic than ferrous complexes and hydroxylation of the cations occurs on very distinct ranges of pH, as indicated by the speciation diagrams.

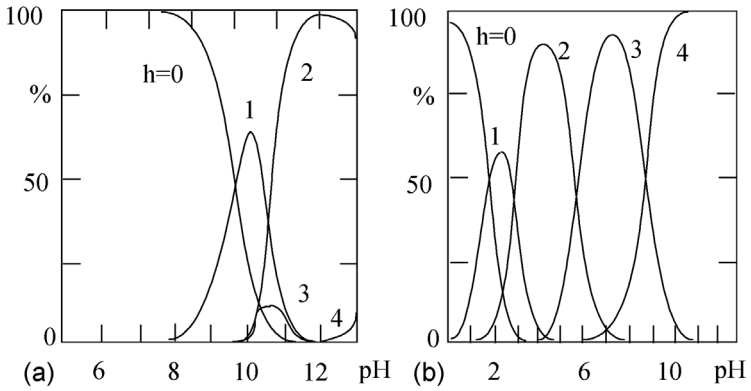

Figure 2: Speciation of $[Fe(OH)_h(OH_2)_{6-h}]^{(z-h)+}$ complexes of (a) Fe(II) ; (b) Fe(III). Reprinted with permission from ref *[15]*. Copyright 2004 Royal Society of Chemistry.

The hydroxylation ratio, h, of a complex increases when the pH increases and aquohydroxo or oxohydroxo complexes are formed. In general hydroxylated cations monomers are instable in

solution. They spontaneously condense because of the nucleophilic character of the OH^- ligands and the electrophilic character of cations.

Depending on the nature of the coordination sphere, two basic mechanisms, of the cations, are proposed for the condensation of hydroxylated complexes.*[19]* Aquohydroxo complexes condense through a nucleophilic substitution which proceeds by the increasing of the coordinence number of the hydroxo ligand and elimination of water molecules. This mechanism is called olation :

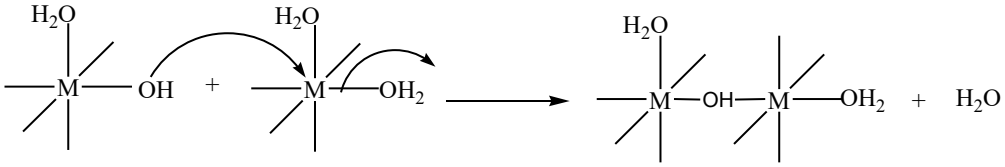

For oxyhydroxo complexes, there is no water molecule in the coordination sphere of the complexes and therefore no leaving group. The condensation mechanism proceeds in that case via two steps:

- At first, association of the oxohydroxo complexes

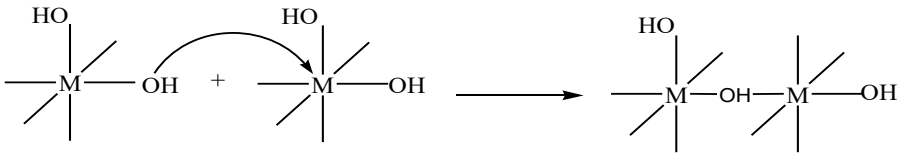

- And then elimination of water molecule and formation of oxo bridges.

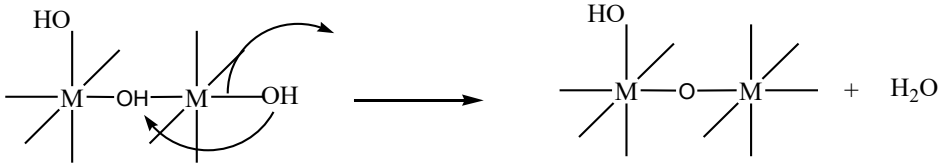

As long as charged complexes exist in solution, the condensation is limited and polycationic species of 10 to 20 cationic atoms are formed. For iron complexes, which are very reactive, ferric species condense very rapidly as soon as pH ≥ 1 and it is difficult to isolate polycationic species. On the contrary ferrous complexes condense only above pH 6 so that some ferrous polycationic species have been isolated. When only zero-charge complexes exist, the condensation is unlimited and a solid phase precipitates:

$$n\,[\,M(OH)_z(OH_2)_{N-z}]^0 \longrightarrow [\,M(OH)_z]_n + n\,H_2O$$

The precipitation is accompanied by the elimination of all the coordinated water molecules and results in the hydroxide formation. When the precipitated hydroxide is unstable it dehydrates spontaneously to form oxides and oxihydroxides. For example, alkalinisation at room temperature of an aqueous solution of ferric ions leads quasi instantaneously to a poorly

defined highly hydrated phase called ferrihydrite. Depending on the pH of the solution the ferrihydrite suspension evolves either to the oxihydroxide phase α-FeOOH (goethite) or to the oxide phase α-Fe_2O_3 (haematite).

2.2 Kinetic steps for the precipitation process.

In order to understand why the precipitation leads to the formation of nanometric particles and how microfluidics can be used as a tool to elucidate the nanoprecipitation mechanisms, we examine in this section the kinetics of the polycondensation process.

We refer to the solid precursor as the zero charged complex $\mathbf{[Fe(OH)_z(OH_2)_{N-z}]^0}$ obtained by hydroxylation of the iron salt solution by an alkaline solution, as we introduced previously. In the following, we abbreviate the zero charged complexes by **P**.

Three steps are usually considered to describe solid particles formation: nucleation, growth (primary growth) and aging (secondary growth). Nucleation can be homogeneous nucleation, heterogeneous nucleation or secondary nucleation.*[20]* We consider here the simpliest case of a homogeneous nucleation, also called classical nucleation theory (CNT), which occurs in the absence of a solid interface and consists in combining solute molecules to produce nuclei.

This step leads to the formation of small clusters with a number of iron atoms sufficiently large to overcome the nucleation barrier The global rate of such a process can be written as $v = k\,[\mathbf{P}]^{\alpha}$, where the values of α can range between 4 and 10, as proposed by Nielsen. *[16]*. These high α values, mean that the nucleation process is not an elementary reaction but the result of many chemical elementary steps.

As the concentration of the precursor **P** generated by hydroxylation increases, and possibly reaches a critical concentration, the condensation rate increases, leading to the formation of many nuclei. This induces a decrease of the precursor concentration and of the condensation rate which can be annulled if the concentration of **P** is very low. As for any chemical process, the driving force behind the homogeneous nucleation is the total free energy of the supersaturated solution ΔG. The overall free energy of the nucleation phenomena can be written as $\Delta G = \Delta G_1 + \Delta G_2$, where ΔG_1 is the volumic contribution, resulting from the difference between the chemical potential of ions in the nuclei (μ_{Pn}) and in solution (μ_P) and ΔG_2 is the contribution of the interfacial energy (γ) when a solid-liquid interface of surface area (A) is created.*[20]*

If we suppose that the global reaction leading to a nuclei formation from P precursors is:

$$pP \Leftrightarrow P_p$$

then ΔG_1 and ΔG_2 can be written as

$\Delta G_1 = p\,(\mu_{Pn} - \mu_P) = -p\,R\,T\,LnS$ and $\Delta G_2 = \gamma\,A$

S is called the "supersaturation", which represents the ratio of the precursor concentration in the solution to the solubility C_b of the macroscopic (bulk) solid i.e $S = [P] / C_b$.

Spontaneous nucleation can occur if S >1 ($\Delta G_1<0$), while no nuclei can form when S<1 ($\Delta G_1>0$). However even if S>1, the nuclei can disappear if their size is not sufficient to overcome the energy barrier due to the competition with interfacial energy ΔG_2.

$$\Delta G_2 = \gamma\, p^{2/3}(36\pi \bar{v}^2)^{1/3} \qquad —$$

The total free enthalpy is thus : $\Delta G = -pRTLnS + \gamma p^{2/3}(36\pi \bar{v}^2)^{1/3}$

The variation of the total free enthalpy with respect to p reaches a maximum when $\partial(\Delta G)/\partial p = 0$. This allow to define a critical number of precursor molecules p*, a critical spherical radius r* beyond which the growth of nuclei is spontaneous, and the energetic barrier that the system should overcomes to reduce its surface energy and to minimise the total free energy ΔG, ΔG^*

$$p^* = \frac{32\pi \bar{v}^2 \gamma^3}{3(RTLnS)^3}; \quad r^* = \frac{2\bar{v}\gamma}{RTLnS} \text{ and } \Delta G^* = \frac{16}{3}\frac{\pi \bar{v}^2 \gamma^3}{(RTLnS)^2} = \frac{p^*}{2} RTLnS$$

From the above equations, it follows that the higher the saturation ratio S is, the smaller the critical nuclei size r* will be and the higher is ΔG^*. Indeed, for a given value of S, all particles with r > r* will grow and all particles with r < r* will dissolve. Figure 3 illustrates this thermodynamic approach for the nucleation process for several cases of supersaturation.

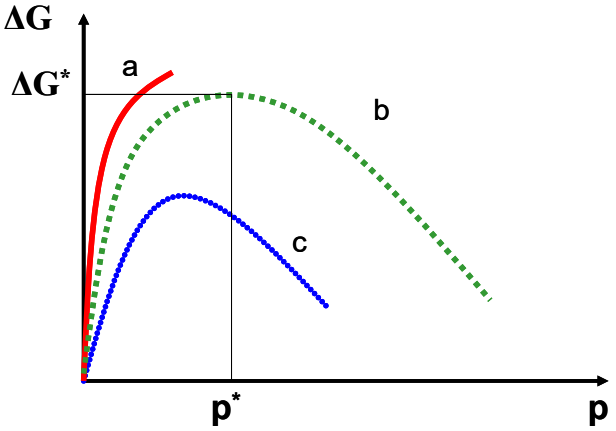

Figure 3 : illustration of the overall free energy ΔG as a function of the number of the precursors p in the nuclei. a : S< 1; b and c : S > 1 and $S_c > S_b$

When the concentration of the precursor reduces below the minimum concentration for nucleation, the latter stops, whereas the growth continues until the saturation equilibrium concentration of the precipitated species is reached (*i. e.* the solubility C_b of the bulk solid). In the classical ion mediated crystal growth, growth occurs by addition of soluble species on the solid phase. The uniformity of the size distribution can be achieved through a short nucleation period that generates all of the particles obtained at the end of the nucleation followed by a self-sharpening growth process. At this stage the system is under kinetic control, the smaller particles grow more rapidly than the larger ones because the free energy driving force is larger for smaller particles than for larger ones if the particles are slightly larger than the critical size r. Figure 4 shows the variation in the precursor concentration with time during the precipitation, in the ideal case when growth successively follows the nucleation step. This is the famous model proposed first by LaMer and Dinegar to explain the mechanism of formation of sulfur sols. *[21, 22]* But in most systems, depending on the concentration of the precursor and on the relative rates of the precursor formation and of the nucleation, nucleation and growth can occur successively or at the same time.

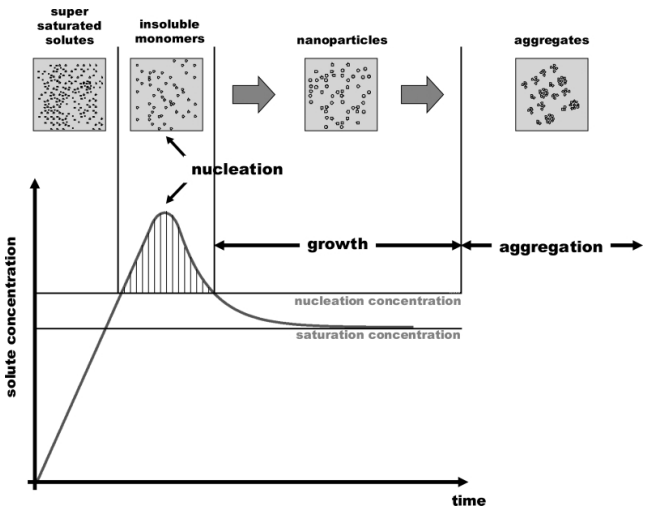

Figure 4: Cartoon illustration of nucleation and growth during the preparation of monodisperse nanoparticles. Reprinted with permission from ref*[23]*. Copyright 2004 Royal Society of Chemistry.

Ideally, a requirement to achieve the monodispersity of the nanoparticles is that nucleation and growth are separated, in time or in space (in separate vessels). In practical, nearly monodisperse size distribution can be obtained by stopping quickly the nucleation-growth

(thermal quench or by supplying a reactant source to keep saturated conditions during the whole reaction *[24]*.

Growth processes are traditionally referred to as ripening or coarsening. Two primary growth mechanisms, illustrated by figure 5, are commonly active to varying degrees during the ripening process.*[25]* In the first growth mechanism, known as Ostwald ripening, larger particles grow at the expense of smaller ones, which are less stable because the solubility of a particle is dependent on its dimension based on the Gibbs-Thomson equation.*[26]*

$$C_r = C_b \exp\left(2\sigma V_m / rRT\right)$$

where C_r and C_b are the solubility values respectively of the nanocrystals and of the corresponding bulk solid respectively, σ, the interfacial tension, V_m , the molar volume of the materials, r, the particles radius, R, the gas constant and T, the temperature. The coefficient $2\sigma V_m / RT$ called "capillary length" is usually of the order 1 nm.*[27]* The solubility based on the Gibbs-Thomson equation describes the solubility of colloidal particles whose radius is larger than ca. 20 nm. For NPs with r = 1 – 5 nm the value of the capillary length is approaching the particle radius and the particle solubility $\mathrm{Ln}(C_r)$ becomes strongly nonlinear against r^{-1} *[28]*, presumably because the interfacial tension σ for a particle with a small number of atoms can no longer be approximated by the value of the macroscopic solid phase. In addition, nothing requires that the nuclei are made of the thermodynamically stable crystalline phase; they could be made of an amorphous phase or of a metastable allotropic phase as well.

The kinetics of Ostwald ripening crystal growth can usually be described by the following power law.*[29]*

$$D(t) = D_0 + k \cdot t^{1/n}$$

where D_0 is the initial particle size (diameter), $D(t)$, the size at time t, k, a rate constant for the limiting step. The exponent, n, is determined by the nature of the rate limiting step. It is equal to 1 when the rate of the growth is controlled by diffusion in solution, equal to 2, when it is controlled by diffusion at the particle surface, equal to 3, when is corresponds to the interface dissolution/precipitation step.

In the second growth mechanism, known as Smoluchowski ripening, particles grow by coalescence through convection or active mixing.

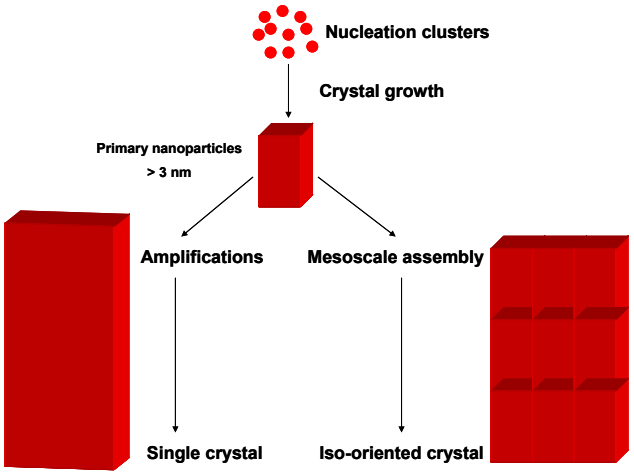
Nucleation clusters
Crystal growth
Primary nanoparticles
> 3 nm
Amplifications
Mesoscale assembly
Single crystal
Iso-oriented crystal

flow, an almost linear relation exists between the position in the reactor and the time.*[40]* A direct observation of the reaction mixture in several points of the reactor, if any suitable detection method is available, provides information about the kinetic of the nucleation and growth processes.*[41]* Mixing and observing in the same time will reduce the dead time that is, even for high efficient mixers, very long compared to the speed rate of precipitation reactions. Mixing in continuous flow microreactors operating under laminar flow occurs by diffusion of the species at the point of confluence.*[42]*

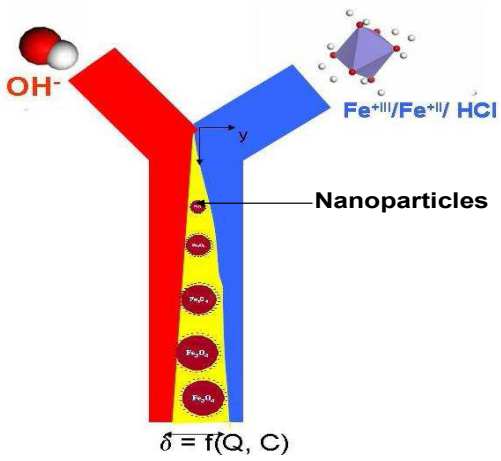

Figure 6: Cartoon showing a typical Y shape continuous flow microfluidic reactor operating under laminar flow, where the reagents mix by diffusion. At the interface nanoparticles nucleate and grow.

Compared to bulk chemistry, where mean concentrations are used to describe the chemical system, chemistry in laminar flows needs to account for local species concentration and their resulted gradients. In the case of the nucleation process, a local precursor concentration can be defined in every point of the reactor giving rise to a local supersaturation and than to different nucleation phenomena. It means that different nuclei with different size will be formed depending on the local conditions. This normally should favourite the increase of the nanoparticles polydispersity, unless a fast mixing of the reagents can occur, creating a burst nucleation followed, or not by a fast growth.

Anyway, microfluidics appears as a versatile tool in order to screen the effect of several parameters on particles size and shape. Indeed mixing and residence times can be easily manipulated.

2.3 Case of magnetite and maghemite nanoparticles

Numerous bulk chemical methods can be used to synthesize magnetic nanoparticles: coprecipitation of iron salts,*[43-46]* sol-gel synthesis,*[47]* hydrothermal reactions,*[48]* hydrolysis and thermolysis of precursors,*[49]* synthesis in microemulsions,*[50]* flow injection synthesis,*[51]* and electrospray synthesis.*[52]*. Contrary to the case of silica or titania, for which a large variety of organometallic precursors exist, providing a good control on the precipitation kinetic, organometallic iron precursors are less abundant and highly reactive; synthesis involving these precursors cannot thus be used for the synthesis of iron oxide particles.

Until now the only one process that has been extended to microfluidics for the synthesis of magnetic nanoparticles is the most used technique in bulk chemistry, i.e. coprecipitation of ferrous and ferric salts in alkaline medium. . As polyol processes and thermal decomposition processes can be easily (with some conditions) extended to microfluidics, they will also be discussed here.

2.3.1 Coprecipitation

Coprecipitation is a facile and a convenient way to synthesize iron oxides (either Fe_3O_4 or γ-Fe_2O_3) in water from a stoechiometric aqueous Fe^{2+}/Fe^{3+} salt solutions by addition of a base under inert atmosphere at room temperature or elevated temperature. The chemical reaction of Fe_3O_4 formation may be written as:

$$Fe^{2+} + 2Fe^{3+} + 8OH^- \longrightarrow Fe_3O_4 + 4H_2O$$

This procedure is in fact a polycondensation process, with its nucleation and growth steps. Quantitative data on nucleation and growth of hydrous metal oxides or hydroxides are rather limited. The reason is that during the precipitation of the solids, competing reactions such as hydrolysis, condensation and anion coordination take place concurrently. The elucidation of the processes is even more difficult when several solute complexes become involved in solid phase formation.*[53]* In the case of iron oxides as magnetite and maghemite, due to the high reactivity of Fe (II) and (III), fast hydrolysis and condensation occur, leading to concurrently nucleation and growth (primary and secondary) and thus to wide size distribution.

According to thermodynamics of the precipitation reaction, complete precipitation of Fe_3O_4 should be expected at a pH between 8 and 14, with a stoechiometric ratio of 2:1 (Fe^{3+}/Fe^{2+}) in a non oxidizing media.*[54]* Experimental results show that the size, shape and composition of the magnetic nanoparticles very much depend on the type of anions associated to the ferric and ferrous cations (e.g. chlorides, sulfates, nitrates), on the molar ratio (Fe^{3+}/Fe^{2+}), the reaction temperature, the pH value and ionic strength of the synthesis medium.

Magnetite Fe_3O_4 nanoparticles are sensitive to oxidation. Magnetite evolves into maghemite γ-Fe_2O_3 in the presence of oxygen. The latter is chemically stable in alkaline and acidic medium. During oxidation of magnetite to maghemite, various electron or ion transfers are involved depending upon the pH of the suspension. Oxidation in alkaline conditions, involves the oxidation of the particles surface, while under acidic and anaerobic conditions, surface Fe^{2+} ions are desorbed as hexa-aqua complexes in solution. Rapid and complete oxidation can be achieved in acidic medium, as described by Massart et al.*[13]*

The main advantage of the coprecipitation process is that a large amount of nanoparticles can be synthesized, without any surfactant. However, achieving by this process a narrow particle size distribution without performing any size sorting is still a challenge.

The first controlled preparation of superparamagnetic iron oxide particles by alkalinisation of an aqueous mixture of $FeCl_3$ and $FeCl_2$ salts was performed by Massart.in the 80th.*[12]* The synthesized nanoparticles were roughly spherical and XRD measurements showed a diameter of 8 nm. Different parameters of this process were largely studied to demonstrate the influence of the pH value, the base (ammonia, CH_3NH_2 and NaOH), of added cations [$N(CH_3)_4^+$, $CH_3NH_3^+$, Na^+, Li^+, K^+, and NH_4^+] and the Fe^{2+}/Fe^{3+} ratio, denoted x, on the coprecipitation yield, the diameter and the polydispersity of the nanoparticles. By modulating the different parameters, magnetic nanoparticles with a mean diameter ranging between 16 to 4 nm were prepared with a good reproducibility.*[13]*The same kind of results were obtained by Vayssières et al.*[55]* and by Jolivet et al.*[54, 56-58]*. The latter explained the shape tailoring by the variation of the electrostatic surface density of the nanoparticles determined by the chemical composition of the crystal surface, the pH and the ionic strength. Babes et al.*[59]* investigated the effect of iron concentration and of the molar ratio x. When x increased, the mean particles size increased but the synthesis yield decreased.

The particles synthesized by Massart's process have been coated by a wide range of molecular species such as amino acids, α-hydroxyacids (citric, tartric, and gluconic acids),*[60]* hydroxamate (arginine hydroxamate),*[61]* dimercaptosuccinicacid (DMSA),*[44, 62]* or phosphoryl choline.*[63]* Bee et al.*[45]* investigated the effect of the concentration of

citrate ions on the size of maghemite particles synthesized by Massart's process. Increasing the amount of citrate ions allows for a decrease in the diameter of citrate coated nanoparticles from 8 to 3 nm. The authors explained these results by the chelation effect of the citrate on the ferric and ferrous cations, preventing nucleation, and by the adsorption of citrate on the nuclei, inhibiting the growth of the latter. Also the authors took benefits from the adsorbed citrate species in order to stabilise the nanoparticles in aqueous dispersion at neutral pH *[64]* The effect of citrate during the synthesis of iron oxide was also studied by Liu and Hang.*[65]* The cristallinity of the synthesised nanoparticles decreased when the concentration of citrate was increased during the synthesis, and the presence of citrate induced changes in the surface geometry of the nanoparticles. In the same kind of idea, Barker et al.*[25]* showed that by capping the magnetite nanoparticles during the synthesis with heptanoic acid in trioctylamine solvent, they were able to slow the repining process thus, reducing the defects in the nanoparticles.

Thus, the size and shape of the nanoparticles can be tailored by adjusting the pH, the ionic strength, the temperature, the nature of the iron salts, the Fe^{2+}/Fe^{3+} molar ratio or by addition of chelating organic anions (caboxylate, citric, gluconic or oleic acid).

But other factors as the mixing rate or the mixing manner can also affect particles size and polydispersity. For example a decrease of the size as well as in the polydispersity is observed when the base is added into the aqueous solution of metallic salts as compared to the opposite process were the iron salts solution is added to the alkaline solution. *[13]* Surprisingly, injection flux rates do not seem to have a preponderant influence on the nanoparticles synthesis.*[59]*

For magnetite nanoparticles, there were much more studies on the growth mechanism and its consequences on the magnetic properties than on the nucleation step.

In the case of iron oxihydroxide particles, dissolution-crystallization plays an important role in the growth mechanisms. It depends on several parameters such as particles size, pH, ionic strength, presence of additives, etc… Different values are provided for the solubility products (K_s) of the several iron oxihydroxides, according to the authors. This may be due to differences in the particles characteristics (size, shape, surface state...). In general the K_s values of the different iron oxihydroxides ranges from 10^{-44} to 10^{-34}.*[3]* Concerning the Fe_3O_4 solubility, there are in fact a large discrepancies in its solubility especially in alkaline medium.*[66]* This is due, probably to the dissolution mechanism which involves the reduction of Fe^{III} to Fe^{II}.*[67]* As a result, the solubility is a function of the reduction potential of the

system which is a real problem under alkaline conditions as dissolved O_2 is an extremely oxidizing agent and kinetic effects may be important.

Ferrihydrite precipitation and aging in solution illustrates nicely how pH controls the solubility and thus the mechanisms of evolution of a population of nanoparticles in suspension. The evolution of the small amorphous nuclei of ferrihydrite obtained by alkaline precipitation of iron (III) salts (nitrate, chloride…) strongly depends on pH (thus on solubility): in the range $5 \leq pH \leq 8$, the insoluble ferrihydrite germs transforms by *in situ* dehydration and local rearrangement into very small acicular particles of haematite α-Fe_2O_3, whereas for a higher solubility in acidic ($pH < 4$) or alkaline ($pH > 8$) media, the transformation proceeds more easily via a dissolution-crystallization process, leading to large goethite needles.

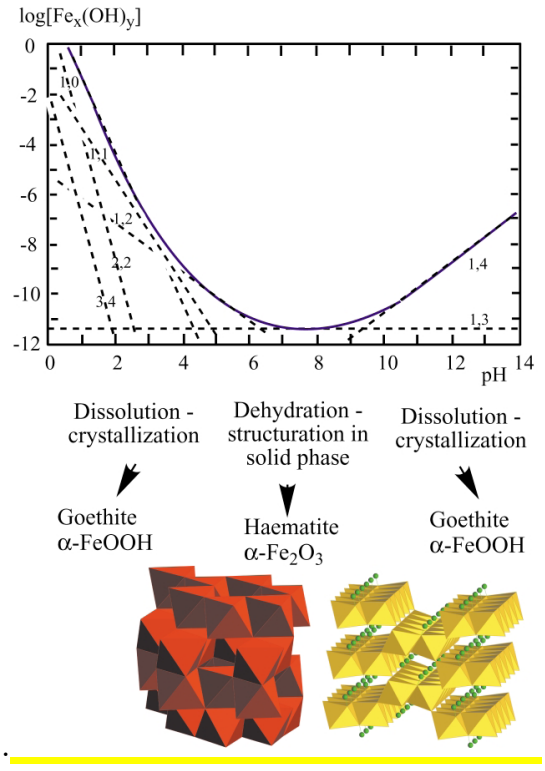

Figure 7: Influence of pH on the solubility of iron and ferric (hydro) oxide crystal structure. Reprinted with permission from ref *[15]*. Copyright 2004 Royal Society of Chemistry.

It seems that Ostwald ripening and coalescence are both involved in the growth of the magnetite nanoparticles. Vayssières et al.*[55]* showed that the size of magnetite precipitated in aqueous solution can be adjusted and stabilized against ripening by controlling the pH and the ionic strength, the latter being imposed by a noncomplexing salt in the precipitation medium.

2.3.2 Thermal decomposition

Decomposition of organometallic compounds in high-boiling organic solvents containing stabilizing surfactants is a procedure that has been widely used to produce magnetic nanoparticles because the latter are obtained with high level of monodispersity and size control. The iron organic precursors are $[Fe(acac)_3]$ (acac = acetylacetonate), $Fe(Cup)_3$ (Cup = N-nitrosophenylhydroxylamine, $C_6H_5N(NO)O^-$), or $Fe(CO)_5$. Hexadecylamine, oleic acid, and fatty acids are often used as surfactants. The size and morphology of the nanoparticles can be controlled by adjusting the reaction times, as well as the aging period, the temperature, the concentration and ratios of the reactants, the nature of the solvent, of the precursors, and the addition of seeds. The decomposition of iron pentacarbonyl $Fe(CO)_5$ in a mixture of octyl ether and oleic acid and at 100°C, followed by oxidation by trimethylamine oxide $(CH_3)_3NO$ at elevated temperature resulted in the formation of monodisperse maghemite nanocrystals with a size of approximately 13 nm.*[68]* The decomposition of $[Fe(acac)_3]$ in the presence of 1,2 –hexadecanediol, oleylamine or oleic acid in phenol ether, leads directly to the oxides.*[69]* The use of iron(III) chloride salts as a iron source has been proposed for the preparation of magnetic nanoparticles.*[70, 71]* . For details, the reader can refer to the reviews of Tartaj and Sato.*[72, 73]* The nanoparticles obtained by this procedure are dispersible in different organic solvents (hexane and toluene) but not in water, and sophisticated post preparative methods are needed to make these nanocrystals water-soluble.

Until now microfluidic reactors have not been used for this kind of synthesis, but the possibility to manipulate small volumes could be of great interest as soon as the microreactors structure and the volumetric rate flow of the different reagents permit the control of the reaction times and the aging periods of the chemical reactions. Also due to the small dimensions of the channels, a precise control of the temperatures and the temperature gradients could be more precise than in bulk. However even if the thermal decomposition enables the synthesis of monodisperse nanoparticles, this process must be largely improved to be suitable for microfluidic preparation, especially because the different organic solvents usually used in this chemistry, and the high temperatures needed for the decomposition of the precursors, are both incompatible with typical PDMS channels, and will require the use of quartz microreactors. And, even if quartz microreactors can be used, the extension of this chemistry in microchannels has to face the problem of the bubbling of the boiling solvents, and the elimination of effluents (sometimes toxic) resulting from the decomposition of the

organometallic precursors. Finally, even if non-toxic precursors can be used, the generated nanoparticles through this process are dispersible in organic solvents, although the main applications of magnetic nanoparticles nowadays require water-soluble particles, for example for applications in biotechnology.

2.3.3 The polyol process

The polyol process refers to the use of polyols (for example ethylene glycol, diethylene glycol) as solvents for the synthesis of metal or metal oxide nanoparticles. Owing to their high dielectric constants, polyols act as solvents able to dissolve inorganic compounds. They offer a wide range of operating temperature for producing inorganic compounds thanks to their relatively high boiling points,.*[74]* They also play the role of reducing agents to produce the metal particles from the precursor, and of stabilizers, allowing to control the particles growth and prevent interparticle aggregation.*[75]* In this method the metal precursor is suspended in a liquid polyol and the solution is heated to a temperature close to its boiling point. This chemical approach has been described for the preparation of well defined shapes and controlled sizes of oxides nano- and microparticles.*[76-83]*

Cai et al.*[84]* successfully synthesized from $Fe(acac)_3$ magnetite nanoparticles in several polyols (ethylene glycol, diethylene glycol, triethylene glycol and tetraethylene glycol) at high temperatures. The mixture was slowly heated to 180°C first and kept at that temperature for 30 min, then quickly heated to reflux (280°C) and kept at reflux for another 30 min. Joseyphus et al.*[85]* reported the synthesis of Fe nanoparticles in polyols, their magnetic properties and the influence of polyols nature on the formation of Fe nanoparticles, but no precisions on the temperature gradients nor on the final temperatures were given by the authors.

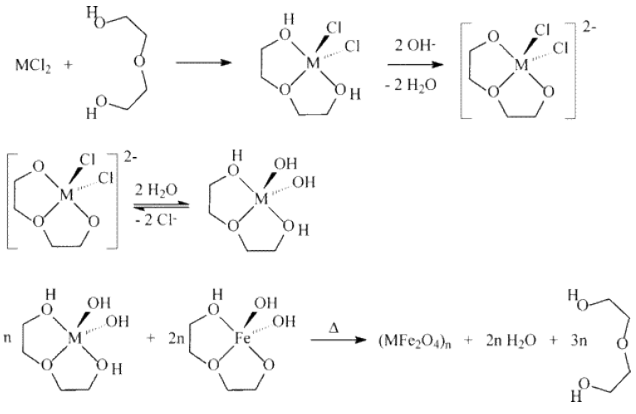

Figure 6: Formation of metal chelated complexes and their decomposition yielding colloidal transition metal ferrites. Reprinted with permission from ref*[86]*. Copyright 2004 American Chemical Society.

Caruntu et al.*[86]* described a new method of synthesis of nanocrystalline iron(II,III) oxide, based on the elevated temperature hydrolysis of chelate ion alkoxide complexes in solutions of corresponding alcohol, diethylene glycol (DEG) and N-methyl diethanolamine (NMDEA).

The polyol processes seem easy and efficient for the synthesis of iron and iron oxide nanoparticles, but all the publications describe the manipulation and control of temperature and temperature gradients. This control can be facilitated by using microfluidic reactors due to the high surface to volume ratio. But at the same time, if a polyols process has to be transposed in microreactors; one has to account for several important points. The precursor and the polyol have to be chemically compatible with the reactor materials, which must also accept the high boiling temperatures needed for this procedure as in the thermal decomposition of metal complexes.

2.3.4 Synthesis in constrained environments

Due to the importance to produce magnetic monodisperse nanoparticles, numerous methods were developed to obtain nanoparticles of more uniform dimensions and well defined size inside constrained environments. These constrained environments include reversed micellar structures of surfactants in nonpolar solvents,*[87-89]* vesicles,*[90]* dendrimers,*[91]* and cyclodextrins,*[92]* etc…

Here we present a few examples of the synthesis in reverse micelles as they are based on the same idea as the digital microfluidics, opposite to the synthesis in direct micelles, using surfactants for which the counter-ion is the metallic cation.*[93]* This idea is that the imprisonment of the reactions in small micro/nanoreactors can impose kinetic and thermodynamic constraints on particle formation and provide a confinement that limits particle nucleation and growth. *[90]*

The first synthesis of magnetic nanoparticles in micelles were reported by Inouye et al.*[94]*who prepared γ-Fe_2O_3 and Fe_3O_4 by oxidation of Fe^{2+} salts. Recently, Lee et al.*[95]*described the use of the reverse micelles technology for the large scale synthesis of uniform and highly magnetic nanocrystals. The particle size is tuned by varying the relative proportion of the iron salts, the surfactant and the solvent. Vidal-Vidal et al presented one-pot microemulsion method to produce monodisperse and coated small nanoparticles. The nanoparticles were formed by the coprecipitation reaction of ferrous and ferric salts with two organic bases, cyclohexylamine and oleylamine into a water-in-oil microemulsion. As final

example, the sythesis of magnetic nanoparticles inside phospholipidic vesicles were reported in the literature (magnetovesicles). Magnetoliposomes of 25 nm were prepared directly using the phsopholipid vesicle encapsulating Fe^{II} ions. The slow diffusion of the hydroxide ions inside the vesicles causes the formation of magnetic nanoparticles.*[90]*

3. Microfluidic synthesis of iron oxihydroxides nanoparticles.

γ-Fe_2O_3 superparamagnetic iron oxide nanoparticles have been prepared for the first time by our group in a continuous coaxial flow microreactor that achieves small diffusion distances and fast mixing times.*[1]* In the same year Frenz et al*[96]* reported the use of droplets-based microreactor for the synthesis of γ-Fe_2O_3 nanoparticles. Later on, the initial coaxial flow setup was improved by separating a nucleation reactor from an aging reactor in order to synthesize another iron oxide, the antiferromagnetic goethite nanolaths α-FeOOH.*[97]* the aim of this section is to review the different methods used for the preparation of these nanoparticles in microfluidics reactors.

3.1 Synthesis of γ-Fe_2O_3 nanoparticles in microfluidic reactors.

3.1.1 Synthesis in continuous flow microreactor

As previously introduced, there are several processes for the synthesis of magnetic nanoparticles. Among them, only coprecipitation has been transposed in microreactors, certainly because reactions occur in aqueous solution, at room temperature. It allows using of PDMS microreactors without any sophisticated chemical engineering. The chemical reaction summarizing the synthesis of magnetite nanoparticles is:

$$Fe^{2+}_{(aq)} + 2\ Fe^{3+}_{(aq)} + 8OH^{-}_{(aq)} \rightarrow Fe_3O_{4(s)} + 4H_2O_{(l)}$$

The first trials of the synthesis were run in a typical two dimensional Y or T shaped microreactors, made by lithography in Polydimethyl Siloxane (PDMS, Sylgard 184). In such microreactors, even when the concentration and the contact times of the different reagents were varied, a magnetic precipitate appears at the interface, and clogs the channels, leading to uncontinuous synthesis process. Clogging is probably due to the adsorption of the magnetic

nanoparticles, which are in contact with the PDMS walls on the top and the bottom of the 2D channel.

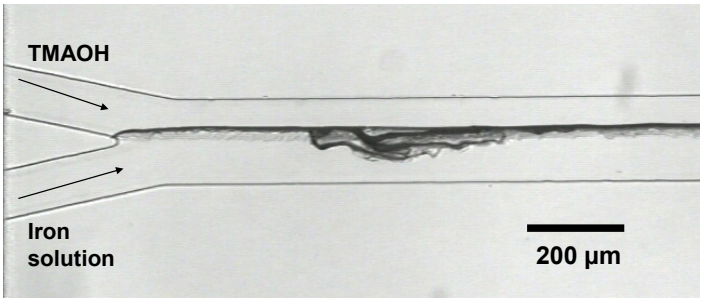

Figure 7: Synthesis of magnetic nanoparticles inside a 2D, Y microreactor showing the clogging at the interface. In a typical test, a solution of total iron salts with different concentrations and 0.5 as molar ratio Fe(II)/Fe(III) was injected in one microreactor arm and a solution of the alkaline solution tetramethylammonium hydroxide ($(CH_3)_4NOH$, TMAOH) in the other arm.

To avoid the technical problems of adsorption and clogging, a 3D coaxial flow microreactor performing the mixing of two coaxial flows of miscible fluids one containing the iron "precursor salts", the other one a strong base, has been designed. It offers the opportunity to enable a precision positioning of the precursors flow at the centre of the channel in both longitudinal and lateral dimensions and on the other hand, it avoids adsorption of any precipitate species onto the PDMS walls as the latter are totally wetted by the alkaline outer flow.*[1]*

The length of the capillary from the confluence region to the outlet was 3cm. A (poly) tetrafluoroethylene (PTFE) tube (500µm ID and 10cm long) leading to a sample vial was connected to the reactor outlet. Depending on the two flow rates Q_{in} and Q_{out}, the residence times ranged between 10 and 48 sec. The outer capillary with 1.7mm diameter (d) was shaped by the molding of a cylindrical tubing (Upchurch Scientific) in a Petri dish with Polydimethl siloxane (PDMS, Sylgard 184) and subsequent removal when the resin is cured. The central capillary with 150µm of inner diameter (I.D.) , 360 µm of outer diameter (O.D.) was obtained by fixing a glass capillary (Plymicro®, usually used for Capillary Electrophoresis) inside the tip of a micropipette (Gilson), which conical shape enables a precise centering.

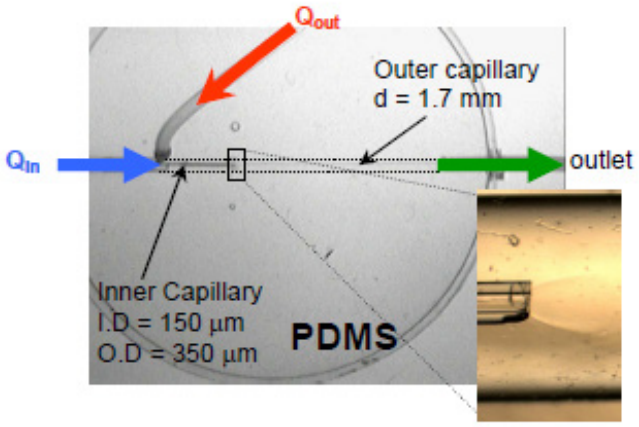

Figure 8: Coaxial flow device operating under laminar regime. The inset image shows the outlet of the inner capillary with the solution of iron +II and iron +III flowing into the stream of TMAOH alkaline solution.

The iron (II/III) solution of total concentration 10^{-2} mol.L^{-1} (Fe(II)/Fe(III) = 0.5) was injected in the inner flow with a volumetric rate flow Qin ($1 < Q_{in} < 100$µl.min^{-1}). The alkaline solution of TMAOH, of a concentration 0.172 mol.L^{-1} was injected in the outer flow with a volumetric rate flow Q_{out} ($100 < Q_{out} < 400$ µl.min^{-1}). TMAOH was chosen prior to any other base as the TMA^+ cations afford enhanced stability of colloidal oxide dispersion.*[43]*

3.1.2 Flow and transport modelling in the continuous flow microreactor

Microreactors' modelling is frequent in chemical engineering to deduce the right hydrodynamic and chemical parameters needed for the chemical synthesis.

The objective of the present section is to describe some aspects of the flow behaviour in the microreactor that are useful for the synthesis of iron oxide nanoparticles. Indeed, there were a few studies on the flow and mass transport in coflow mixers and they reported fundamentally the analytical aspects of mixing under laminar flow, rather than the influence of mixing on the physico-chemical parameters of a reaction. Andreev et al.*[98]* developed a mathematical model to describe the hydrodynamic and mass transfer during an acid base reaction and showed that the maximum of the mean value product is obtained when the inner flow is considerably higher than the outer flow rate. The same group*[99]* studied again, the mixing in a coflow mixer for injection flow analysis and deduced that the mixing time is independent of the total volumetric rate flow Q_{tot} after the point of confluence but depends on the volumetric rate flow ratio of the outer flow to the inner flow α, $\alpha = Q_{out}/Q_{in}$. Mixing times decreased when α was increased

Confocal Laser Scanning Microscopy compared to the numerical model for pH mapping

in the microreactor has been described in details in our submitted work.*[100]* Here we review in brief some of the results important for the synthesis of the nanoparticles.

3.1.2.1 Transport modeling: pH gradients.

Studies in bulk (see paragraph 2) have shown that for the synthesis of high quality magnetic nanoparticles and the good reproducibility of the results, parameters as the ratio Fe(II)/Fe(III) , the pH, the mixing manner, the temperature and others…. need to be controlled ,.

pH is the most important parameter, as it controls the hydrolysis, the polycondensation and then the precipitation of the iron oxides. As Fe(II) and Fe(III) hydrolysis occurs in two different pH ranges, and as Fe(II) absorption is responsible of the magnetic properties of the magnetite,*[18]*, a very fast elevation of the pH (and thus a fast mixing) in the alkaline zone would minimize the formation of non magnetic iron (III) oxihydroxides and increase the yield in magnetic nanoparticles.*[101]*

To understand how the different volumetric rate flows affect the pH gradients in the microreactor, a theoretical approach based on solving the underlying mass transport for the different chemical species in the reactor, coupled to the comparison to experimental images from confocal laser scanning microscopy (CLSM) experiments was performed.

First, as precipitation reactions are complex, the pH variations occurring during the mixing in the microreactor described above due to a model reaction which is the neutralisation of a strong acid HCl by the strong base TMAOH were studied. HCl and TMAOH concentrations being the same as the ones used in the typical chemical synthesis of the magnetic nanoparticles, i.e 0.794 $mol.L^{-1}$ and 0.172 $mol.L^{-1}$ respectively. The experimental methodology consists in using a micromolar concentration of pH dependant dye (fluorescein) in the inner stream containing the HCl solution in order to map the pH changes in the central jet stream where the acid-base reaction proceeds. The experimental results were compared to modelling, the pH distribution in the reactor and the local fluorescein concentration being predicted by modelling the underlying mass transport of the various species in the system.

The evolution of the concentration $C_i = C_i(\mathbf{r},t)$ of solute particles i follows the continuity equation

$$\frac{\partial C_i}{\partial t} + \mathrm{div}(C_i\mathbf{u} + \mathbf{j}_i) = \sigma_i$$

u is the hydrodynamic velocity in the channel, calculated from the Navier-Stokes equation together with the compressibility condition. For a dilute system, it can be identified to the local average velocity of the solvent. $\boldsymbol{\sigma}_i$ is the creation term and represents the local creation rate of particles due to the chemical reactions. $\mathbf{j}_i$ is the diffusive flux of species i. The general expression of the $\mathbf{j}_i$'s can be obtained from non-equilibrium thermodynamics. For a dilute solution, cross correlations are negligible and it reduces to the Nernst-Planck expression :

$$\mathbf{j}_i = -D_i \mathbf{grad} C_i + \frac{D_i}{k_B T} C_i Z_i e \mathbf{E}$$

The electric field **E** is chosen to satisfy the Henderson field condition. Consequently, at any time the charge distribution has the time to relax and the local electroneutrality condition $\sum_i Z_i C_i = 0$ is valid.

The various solute species i are $H^+_{(aq)}$, $OH^-_{(aq)}$, Cl^-, TMA^+ and the fluorescein. Diffusion coefficients were estimated from the values at infinite dilution: D_{H^+} = 9.2 x 10^{-9}, D_{Cl^-} = 2.03 x 10^{-9}, D_{OH^-} = 5.28 x 10^{-9}, D_{TMA^+} = 2 x 10^{-9} $m^2.s^{-1}$.

To simulate the different fluorescein species during the acid-base reaction between HCl and TMAOH, the following assumptions were made: (i) fluorescein is diluted in the hydrochloric acid, so no need to account for its charge. Convection diffusion equation with no chemical reaction can be solved to calculate the local concentration map of the total fluorescein denoted Flu; (ii) Fluorescein is diluted compared to H^+ concentration in the acidified fluorescein solution and cannot interfer during the acid base-reaction; (iii) The different ionic species of the fluorescein have the same diffusion coefficient $D \approx 0.2$ x 10^{-9} $m^2.s^{-1}$.

After calculating the local pH in the microreactor, the convection diffusion equation was solved for the fluorescein dye. Since the acid-base reactions are virtually instantaneous, it has been assumed that chemical equilibriums are locally achieved for the different fluorescein species.

Confocal Laser Scanning Microscopy experiments were used to confirm these modeling results. Fluorescein is a well-known pH sensitive dye, which progressively deprotonates when pH increases, as shown on figure 11, producing the di-anion F^{-2} which is the only

fluorescent species (mono-anion F^{-1} is quite less fluorescent). As the pH rises in aqueous solution, the fluorescence signal increases starting at pH~5 and saturating at a maximum value above pH~7. To verify the pH dependence of the signal, a stock solution of disodium fluorescein was prepared and diluted at 6 µM in different pH-buffered solutions. The solutions were perfused in both the inner and outer capillaries and the corresponding fluorescence images were captured with the CLSM at the median plane of the channel (i. e. far from the walls which produce an artifact due to possible adsorption of fluorescein onto PDMS). The images appeared uniform across a 300 µm x 300 µm view field. By averaging the intensity over this constant area, a calibration plot has been builded up on figure. 11.(b). The results are in good agreement with cited work.*[102]*

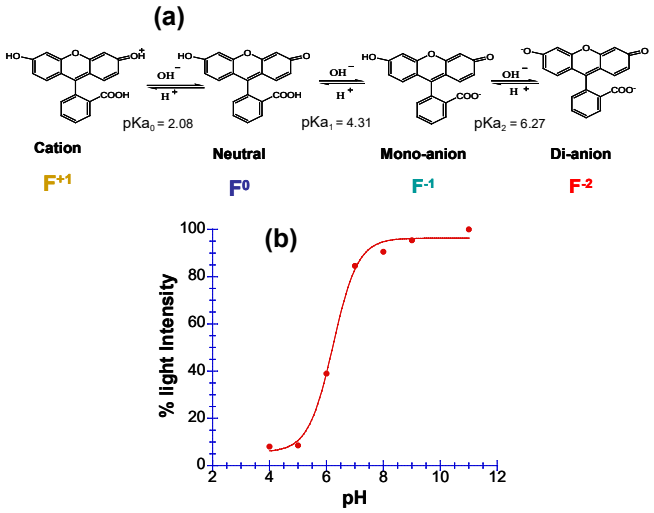

Figure 9: (a) Chemical structures of fluorescein based on different pH. Fluorescein is a cation at pH < 2.08, neutral at 2.08 < pH < 4.31, an anion at 4.31 < pH < 6.27, and a dianion at pH > 6.27. (b) Percentage light intensity relatively to the value at pH 11 as a function of pH for a solution of 6 µM disodium fluorescein.

Figure 12 shows the steady-state 2D fluorescence profile obtained by confocal slicing in the middle of the outlet of the inner capillary where acidified fluorescein solution (6 µM) flows in the centre surrounded by the outer alkaline TMAOH solution upon application of a volumetric ratio $\alpha = 400$

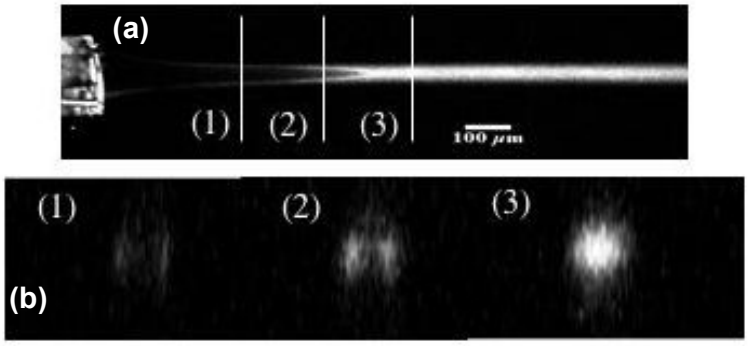

Figure 10 : (a) CLSM image of the acid-base reaction in presence of 6 μM fluorescein solution in the inner flow with an applied volumetric rate flow α = 400. The image was recorded in the X-Y plane. (b) The three images are X-Z images, taken at the locations indicated by (1), (2) and (3), constructed from a "Z-stack". The Z-stack consisted in 20 slices, which were spaced at 20 μm intervals.

The fluorescence burst in the central jet was interpretated as due to the deprotonation of fluorescein by the hydroxide ions diffusing towards the center that remain in excess after reaction with H^+. The hollow cylindrical shape on the fluorescence image (cross-sections (1) and (2) of the central stream) illustrates the transition from a still acidic core (below pH 4) of the stream to a neutralized "skin" near the pKa of 6.2 of fluorescein. It is exactly in this boundary region near the pH equivalence that the coprecipitation of the iron salts in a synthesis experiment is expected.

To illustrate the good agreement between the CLSM experiment and the model, figure 13. compares the 2D fluorescence intensity map of fluorescein represented by a scale from cold (low intensity, acid) to warm colors (high levels, basic). The symmetry between the experimental part of the image on the left and the calculated one on the right is a clear evidence that the assumptions made to calculate the diffusion of the fluorescein species and the acid-base reaction are acceptable.

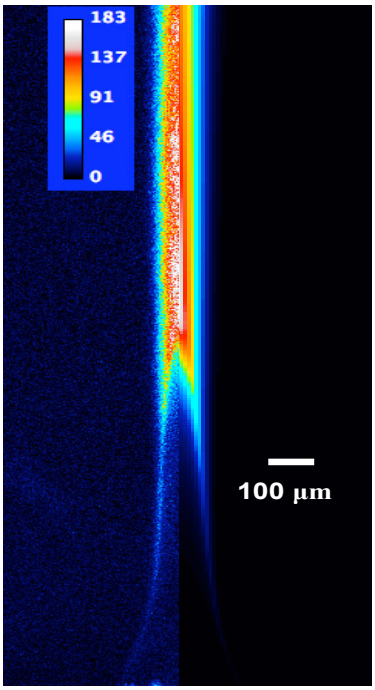

Figure 11: Comparison of the experimental and predicted fluorescence intensities in the X-Y plane with (a) the left half-plane representing the experimental fluorescence intensity and (b) the right half-plane with the predicted fluorescence intensity for $\alpha = 400$.

Finally, the flow rates ratio α was tuned between 40 and 400 and the corresponding fluorescence profiles along the $r = 0$ axis were compared on figure 14.a. The good matching between the predicted and the experimental intensity curves for several values of α clearly validates the proposed simulation method.

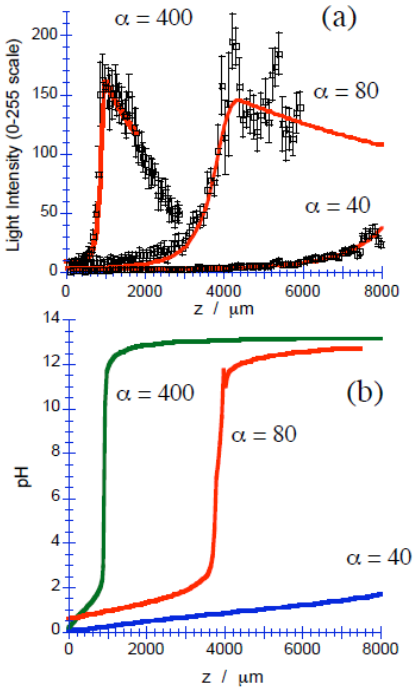

Figure 12: (a) Evolution of the experimental fluorescence profiles (□) when α = 40; 80 and 400 along the symmetry axis (r = 0). The lines represent the predicted fluorescence intensities calculated for each case from the simulated F^{-2} concentrations, (b) Simulated pH profiles along the symmetry axis (r = 0) for α = 40; 80 and 400

Fluorescein is just a pH reporter dye, and the shape of the pH curves is in good accordance with the titration of a strong acid (HCl) by a stong base (TMAOH). When α increases, the squeezing effect of the inner stream by the outer stream increases; the inner stream containing the fluorescein dye and HCl is focalised, thus OH^- diffusion pathways to the H^+ ions are reduced. This decrease of the diffusion distance between the reagent species implies a faster mixing and a steeper jump of pH near the equivalence point (pH = 7). In view of these results and in order to synthesize magnetic nanoparticles, α = 400 was found to be the best suitable case, because it offers the advantage of a fast mixing and a sharp pH jump . The choices α = 80 and 40 would lead to a decrease of the yield in magnetic nanoparticles due to the precipitation of antiferromagnetic iron hydroxides. These results were used for the preparation of the stable colloidal and magnetic nanoparticles reported in our work*[1]* using the coaxial flow microreactor and that will be resumed in the next section.

3.1.2.2 Application for the synthesis of γ-Fe_2O_3 nanoparticles

For the nanoparticles synthesis experiments, the inner solution was a mixture of iron salts

with a total concentration of ferric and ferrous salts c = 10^{-2} mol.L^{-1} and 0.5 as a molar ratio Fe(II)/Fe(III), prepared by mixing $FeCl_3$ and "fresh' $FeCl_2.4H_2O$ salts in diluted and degased hydrochloric acid (pH ~ 0.10). The outer flow was an alkaline solution of tetramethylammonium (TMAOH, 0.172 mol.L^{-1}) which was injected with an outer volumetric rate flow Q_{out}. The reaction was "quenched" by fast solvant extraction (using didodecyl- dimethyl ammonium bromide in cyclohexane) to prevent any ageing of the nanoparticles in the aqueous solution..

The suspensions obtained in cyclohexane were always stable and the nanoparticles produced in the channel were fairly spherical with an average size around 7 nm. The evidence of their cristallinity was provided by the electron microdiffraction pattern in the inset of figure 15, which shows the presence of the maghemite phase γ-Fe_2O_3.

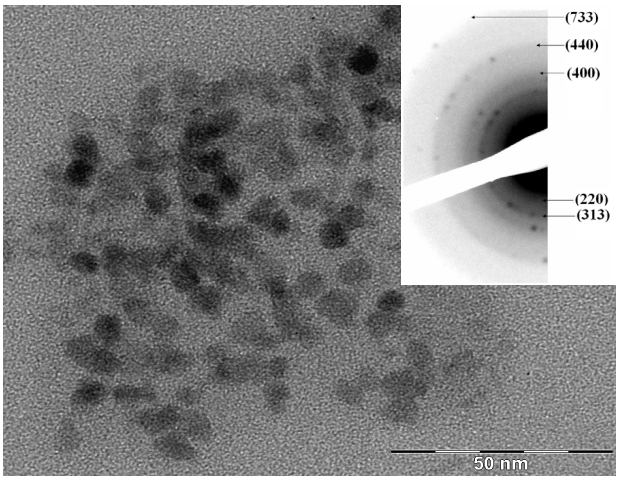

Figure 13 : TEM image of nanoparticles prepared in the channel (for flow rates Q_{in} = 100 µl/min and Q_{out} =400 µl/min). The inset shows the electron microdiffraction pattern with the Miller indices of γ-Fe_2O_3. Reprinted with permission from ref *[1]*. Copyright 2008 Royal Society of Chemistry

Although suspensions obtained in cyclohexane were stable in a zero magnetic field, they sediment in the presence of a magnetic field gradient (for example on a strong permanent magnet), which suggests a magnetic character. This observation was confirmed by magnetization measurements (using a Vibrating Sample Magnetometer) on a stable unquenched (aqueous) suspension: the magnetization curve (figure 16) followed the Langevin law typical of superparamagnetism, calculated for an assembly of nanoparticles with a rather narrow distribution of diameters fitted by a Log-normal law of parameters d_0=6 nm and σ=0.2.

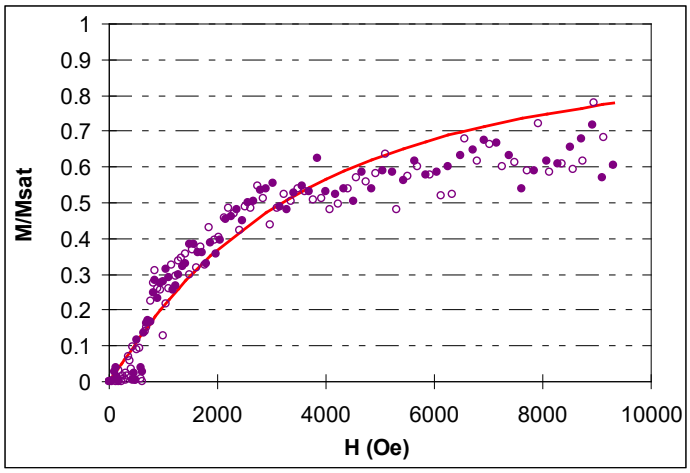

Figure 14: Magnetisation curve of a stable suspension in water of nanoparticles produced in the millifluidic device. The inset curves represent the fitting Log-normal laws for the numbers distribution (solid line) and the volume distribution (dotted line) of diameters. Reprinted with permission from ref *[1]*. Copyright 2008 Royal Society of Chemistry

By measuring both the volume fraction of nanoparticles $\phi=5.7x10^{-5}$ (from iron titration by atomic spectroscopy) and the saturation magnetization M_{sat}= 7.9 A/m for the suspension, the specific magnetization of the materials was deduced $m_s= M_{sat}/\phi=1.4x10^{+5}$ A/m, which is much below the bulk value of maghemite γ-Fe_2O_3 ($3.5x10^{+5}$ A/m), but not so far from the m_s value about $2.6x10^{+5}$ A/m usually obtained for nanoparticles of approximatively the same sizes prepared with the standard large scale synthesis. Therefore it can be deduced that nanoparticles prepared within few seconds in a millifluidic channel exhibit only a small decrease of ordering of their magnetic moments compared to particles obtained within about 30 minutes in bulk.

3.2 Synthesis in microdroplets reactor

The use of a droplets based microreactor for the synthesis of magnetic nanoparticles by coprecipitation of iron(II) and (III) by an alkaline solution of ammonium hydroxide was reported by Frenz et al.*[96]*. The microfluidic device consisted of two hydrodynamically coupled nozzles. During droplet formation in one of the nozzles, the aqueous stream blocks the oil coming from the central channel, leading to an increased oil flow through the second nozzle. Once the droplet is released the oil flow switches back to the first channel, allowing droplet pairing at various flow rates.

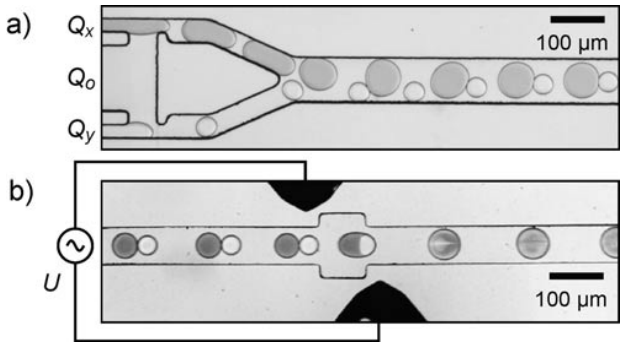

Figure 17: a) Pairing module. Two aqueous phases are injected by the outer channels and are synchronously emulsified by the central oil channel. The flow rates are Q_o=800 mLh^{-1} for the oil and Q_x=400 mLh^{-1}, Q_y=100 mLh^{-1} for the aqueous phases. b) Fusion module. Paired droplets can be coalesced by applying an electrical voltage U between the two electrodes. Q_o=650 mLh^{-1}, Q_x=100 mLh^{-1}, Q_y=60 mLh^{-1}. Reprinted with permission from ref*[96]*. Copyright 2008 Wiley.

Iron chloride solution was flushed into one arm of the nozzle and ammonium hydroxide into the second arm, which led to droplet pairs containing the two reagents. To start a reaction the droplet pairs can be coalesced by applying an electrical field between the two on-chip electrodes.

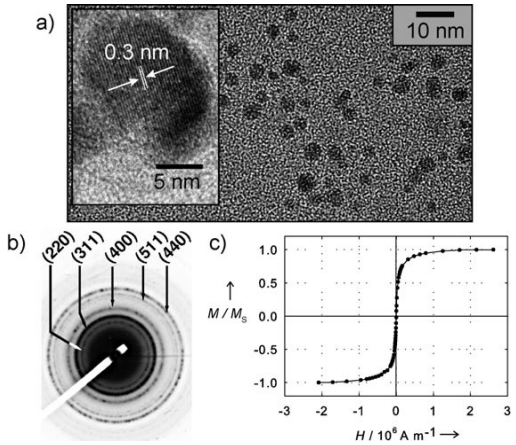

Figure 18: Characterization of the iron oxide particles produced. a) TEM image of the nanoparticles. Inset: HRTEM image of a particle showing (220) spinel planes. b) Electron diffraction pattern indicating different planes of the spinel structure. c) Magnetization M/M_s (M_s is the saturation magnetization) as a function of the magnetic field H. Reprinted with permission from ref*[96]*. Copyright 2008 Wiley.

Transmission electron microscopy and electron microdiffraction pattern showed that synthesized nanoparticles are monocrystalline and that the phase is γ-Fe_2O_3. The average particle size deduced from TEM images is smaller for the fast compound mixing (4 ± 1 nm) than for bulk mixing (9 ± 3 nm). The supeparamagnetic character of the nanoparticles is confirmed by the absence of hysteresis in the magnetization curve.

The authors present their methods as a reliable way to produce magnetic nanoparticles. However this method uses oils and surfactants to achieve the formation of the droplets and their fusion. These “additives” can affect the nucleation-growth mechanisms of the particles.

Compared to microdroplets reactors, continuous-flow reactors are easier to handle and are more representative of the conditions of the bulk synthesis, with improved homogeneity, thus offering a better reproducibility of the synthesized particles. The authors defend their use of microdroplets by the enhancement in mixing by convection and the decrease of the reagent dispersion, due to the droplets which act as spatially isolated microreactors. This concept is in fact the same as the one evoked for the synthesis of nanoparticles inside vesicles or microemulsions.*[93-95]* The faster mixing time reported in this system is 2 ms, which is far larger than the nucleation time . Moreover, this time is difficult to define as it is totally arbitrary and depends on the concentrations of the reagents.

3.3 Synthesis of α-FeOOH nanoparticles in microfluidic reactors.

Another interesting iron oxihydroxide phase is goethite (α-FeOOH) which is widely found in iron-rich soils.*[35]* This clay mineral constitutes the natural ochre pigment, and because of its elongated shape, synthetic goethite is often used as a precursor of α-Fe "hard magnet" particles for magnetic recording.*[103]* Because of this elongated shape, suspensions of antiferromagnetic goethite/plate-like nanostructures (nanolaths) exhibit an original magneto-optical effect, and self assemble spontaneously into a nematic liquid-crystal phase above a threshold concentration.*[104]* The importance of particle shape for the improvement of magnetic properties, or the control of the particle assembly, requires control of the synthetic conditions of these particles.*[105]*

The bulk methods reported for the synthesis of acicular (needle-like) goethite particles are based on the aging of ferrihydrite nanoparticles obtained by alkalinisation of iron(III) salt solutions.*[106]* They are indeed easily transferable to microfluidic devices as illustrated by *[97]*

As discussed former the alkalinisation at room temperature of a solution of ferric salts by an alkaline solution leads to the precipitation of an amorphous oxide hydroxide precipitate of ferrihydrite. At its minimum of the solubility, ferrihydrite can evolve to haematite through an internal dehydration process, while in high solubility domains (very acidic or very alkaline solutions), the transformation via a dissolution-precipitation mechanism is possible and leads to the formation of goethite. Goethite is the most thermodynamically stable phase, but due to the low solubility of iron oxides, the transformation into goethite is very slow, offering the possibility of a good separation between nucleation and growth. Another possible mechanism

for the formation of goethite nanoparticles, is the oriented attachment of iso-oriented ferrihydrite nanoparticles and then crystallisation into goethite nanoparticles.*[107]*

A complex microfluidic device (figure 19) was proposed by Abou-Hassan and al. *[97]* in order to physically separate the process of nucleation of the ferrihydrite nanoparticles from their growth, leading to goethite particles. The nucleation of the primary ferrihydrite nanoparticles is induced by diffusive mixing at room temperature in a microreactor that is based on coaxial flow geometry (R1). This mixing reactor is the same described for the synthesis of the magnetic nanoparticles and is based on a three-dimensional coaxial-flow device of two streaming reagents. At the outlet of this micromixer, the suspended ferrihydrite nanoparticles are directly injected into the microtubular aging coil R2, which consists in a transparent PTFE tube of 1.7 mm inner diameter and 150 cm total length continuously heated in a water bath at 60°C. Temperature profiles were calculated to determine the tubing length (and thus the time) required for the fluid to reach a steady state. At the outlet of R1 (before aging) and R2 (after aging), the resulted suspension is collected and analysed by Transmission Electron Microscopy (TEM) and by High Resolution TEM (HRTEM).

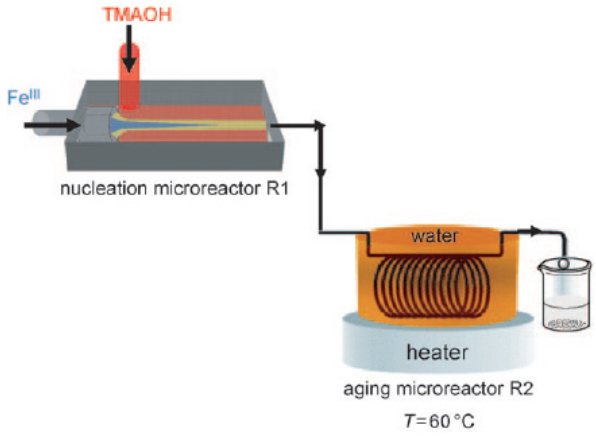

Figure 19: The experimental setup used for the preparation of the ferrihydrite and goethite nanoparticles. TMAOH= Tetramethylammonium hydroxide. Reprinted with permission from ref*[97]*. Copyright 2009 Wiley.

TEM pictures of the particles obtained after R1 show well defined spherical ferrihydrite nanoparticles (nanodots) of about 4 ± 1 nm in size figure 20.a. High-resolution TEM (HRTEM) measurements (figure 20.b) show that the nanoparticles are monocrystalline, exhibiting atomic planes with an interplanar distance of about 2.5 A, which is consistent with ferrihydrite nanoparticles.

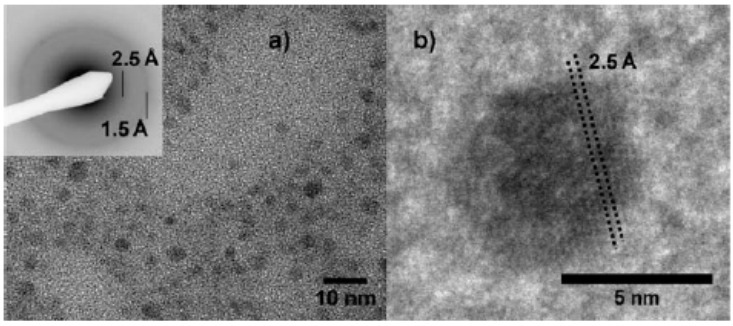

Figure 20: a) TEM picture of the sample taken after precipitation in the microreactor R1 (before aging), showing ferrihydrite nuclei of 4 ± 1 nm diameter. The selected area-diffraction pattern (inset) is typical of two line ferrihydrite. b) HRTEM image of an individual ferrihydrite nanoparticle with a 2.5 Å lattice fringe. Reprinted with permission from ref*[97]*. Copyright 2009 Wiley.

Under the given flow rate, the ferrihydrite solution reaches 60°C in about 1 s, that is, within the first centimeter after it has entered the heated zone of the tubing. The effective residence time is about 15 min, as estimated from the length of the tubing along which the fluid has reached the stationary temperature of 60°C.

After aging for 15 min under continuous flow in the aging coil R2, goethite plate-like nanostructures were observed with an average length L=30 ± 17 nm and width w=7 ± 4 nm (figure 21 a). This short aging time appeared to be sufficient for the growth of crystalline and anisotropic goethite nanoparticles that differ only in smaller sizes compared to those obtained after complete aging (one day at 60°C).*[108]*

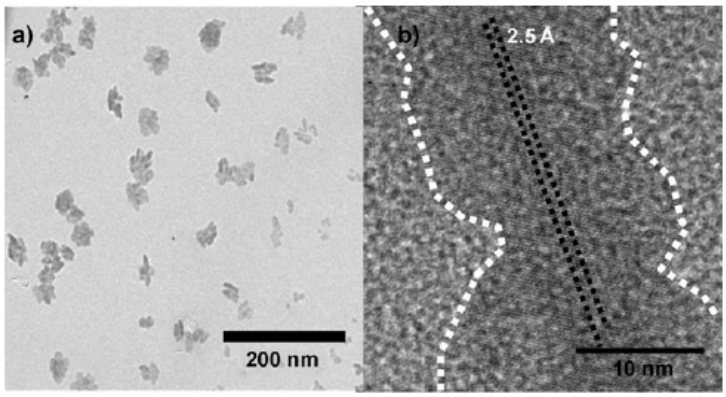

Figure 21: a) TEM image of the nanolaths after aging for 15 min in the microtubular loop R2, produced at pH 13 and under laminar flow. b) HRTEM image of a nanorod particle. Lattice fringe spacing isconsistent with goethite. The dashed lines serve to highlight the morphology and texture of the particle. Reprinted with permission from ref*[97]*. Copyright 2009 Wiley.

Moreover, the presence of few remaining ferrihydrite nuclei undergoing aggregation in the batch after 15 min and even after 24 h at 60°C (data not shown) supports the idea that goethite

nanoparticles were formed by the aggregation mechanism rather than by dissolution/reprecipitation.

Thus the use of microfluidics device allows to significantly accelerate the synthesis of goethite nanoparticles from ferrihydrite nuclei. The novelty of this approach lies in the separation of the nucleation of the primary particles (ferrihydrite) and the growth of the goethite nanoparticles in two independent microreactors operating in different conditions. In the nucleation microreactor, the streaming reagents are mixed by molecular diffusion at room temperature in a flow focusing geometry. The homogeneity of the mixture is ensured by the fast mixing time and the technical difficulty of microchannel clogging owing to precipitation onto the walls is avoided by the 3D geometry. The use of a microfluidic device for aging, by minimizing local temperature gradients, ensures a regular laminar flow, and finally leads to crystalline plate-like nanostructures. These particles have approximately the same values of aspect ratio and polydispersity index than the ones obtained in the bulk synthesis (bulk synthesis usually yields goethite nanoparticles with a typical length of about 250 nm and width of 40 nm, with a polydispersity index of about 50% for both dimensions *[109]*) but are smaller in size. The time required for aging falls down to 15 min (for a velocity of 0.1 $cm.s^{-1}$) compared to bulk synthesis (several hours or days). This may originate from the small diameter of the aging reactor, causing a shear stress that prealigns the primary ferrihydrite nanoparticles and speeds up their oriented aggregation process.

4. Perspectives

Among all the ferric oxide nanoparticles, superparamagnetic ones (SPIONs: SuperParamagnetic Iron Oxide Nanoparticles) are of special interest because of their applications in the field of imagery and therapy. At the present time the screening of the relation properties/structure is not very easy nor economic in bulk and the use of continuous microfluidic systems, providing the ability to add reagents along the entire length of the channel, can be a very useful tool for screening the different parameters (size, surface fonctionnalisation, aggregation) allowing to optimize given properties. This idea is illustrated in the figure .22 and can be summarized by three operations: adding, mixing, and reacting.

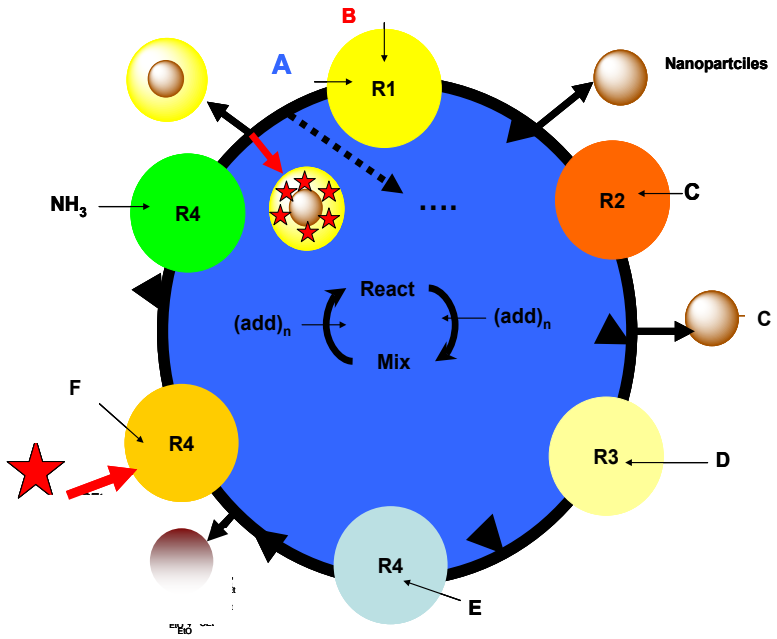

Figure 22: Cartoon illustrating the idea of on-line synthesis of functional nanomaterials.

Indeed, if several microreactors R_i are associated in series together, to form a series of microunit operations, the synthesis of SPIONS nanoparticles and their surface modification would be possible in an unique on-line process. The surface coating of the SPIONS by silica is a good example. Silica has been extensively exploited as a coating material for magnetic nanoparticles.*[110-112]* in order to get a protective, biocompatible, inert, and hydrophilic surface with excellent anchoring points for derivatizing molecules.*[113]* Several methods were reported in the literature for the formation of superparamagnetic iron oxide nanoparticles silica nanocomposites including reactions performed under Stöber conditions,*[114, 115]* microemulsions,*[116]* emulsions,*[117]* and aerosol pyrolysis.*[118]* It seems that core shell SPIONS@Silica nanoparticles and SPIONS@luminescent Silica nanoparticles can be obtained in microfluidic reactors without the use of any surfactant (Abou-Hassan, unpublished results).

In the field of on-chip magnetic separation, there were many works devoted to the separation of micrometric magnetic particles, but to date no separation of nanometric particles on the microfluidic scale has been reported.*[119]* A continuous flow method capable of separating magnetic from non-magnetic particles as well as separating different magnetic particles from each other can be very helpful, in synthetic chemistry.

But the most important challenge in the field of nanomaterials synthesis in microfluidic lies in the development of on-line characterization methods. For quantum dots or metallic nanoparticles, optical characterizations allowing to establish a simple relation with particles

size, are available. That is not the case for ferric oxide nanoparticles. As the latter have magnetic properties, on line magnetic measurements can perhaps be designed. On the same kind of idea, but of course general for any kind of materials, on line characterisations using Small Angle X-ray or Neutron Scattering have to be developed. There are thus important attends in designing on-line nanoparticles characterization techniques.

5. References

[1] A. Abou Hassan, O. Sandre, V. Cabuil, P. Tabeling, *Chem. Commun.* **2008**, 1783.
[2] http://marsrover.nasa.gov/.
[3] R. M. Cornell, U. Schwertmann, *The Iron Oxides: Structure, Properties, Reactions, Occurrences and Uses*, Wiley-VCH, **2003**.
[4] J. L. Dormann, D. Firoani, *Magnetic Properties of Fine Particles*, North-Holland, Amsterdam **1992**.
[5] J. Eisenmenger, I. K. Schuller, *Nat Mater* **2003**, *2*, 437.
[6] J. T. Ferrucci, D. D. Stark, *Am. J. Roentgenol.* **1990**, *155*, 943.
[7] S. Sun, C. B. Murray, D. Weller, L. Folks, A. Moser, *Science* **2000**, *287*, 1989.
[8] M. M. Miller, G. A. Prinz, S. F. Cheng, S. Bounnak, *Applied Physics Letters* **2002**, *81*, 2211.
[9] I. Chourpa, L. Douziech-Eyrolles, L. Ngaboni-Okassa, J. F. Fouquenet, S. Cohen-Jonathan, M. Souce, H. Marchais, P. Dubois, *Analyst* **2005**, *130*, 1395.
[10] M. S. Martina, J. P. Fortin, C. Menager, O. Clement, G. Barratt, C. Grabielle-Madelmont, F. Gazeau, V. Cabuil, S. Lesieur, *J. Am. Chem. Soc.* **2005**, *127*, 10676.
[11] R. Massart, *French Patent 79-188-42* **1979**.
[12] R. Massart, *IEEE Trans. Magn.* **1981**, *17*, 1247.
[13] R. Massart, V. Cabuil, *J. Chim. Physi.* **1987**, *7*, 84.
[14] R. Massart, E. Dubois, V. Cabuil, E. Hasmonay, *J. Magn. Magn. Mater.* **1995**, *149*, 1.
[15] J.-P. Jolivet, C. Chaneac, E. Tronc, *Chemical Communications* **2004**, 481.
[16] A. E. Nielsen, *Kinetics of Precipitation*, Oxford **1964**.
[17] C. f. Baes, R. E. Mesmer, *The Hydrolysis of Cations*, J. Wiley and Sons, New York **1976**.
[18] J. p. Jolivet, *Metal Oxide Chemistry and Synthesis. From solution to solid state*, Chichester **2000**.
[19] J. P. Jolivet, C. Chaneac, E. Tronc, *Chem. Commun.* **2004**, *5*, 481.
[20] D. Kashchiev, *Nucleation Basic Theory with Applications*, Butterworth-Heinemann, **2000**.
[21] V. K. LaMer, R. H. Dinegar, *J. Am. Chem. Soc* **1950**, *72*, 4847.
[22] V. K. LaMer, *Ind. Eng. Chem.* **1952**, *44*, 1270.
[23] A. J. deMello, J. C. deMello, *Lab Chip* **2004**, *4*, 11N.
[24] Q. Zhang, S.-J. Liu, S.-H. Yu, *Journal of Materials Chemistry* **2009**, *19*, 191.
[25] A. J. Barker, B. Cage, S. Russek, C. Stoldt, *Journal of Applied Physics* **2005**, *98*, 063528.
[26] T. Sugimoto, *Adv. Colloid Interface Sci.* **1987**, *28*, 65.
[27] A. S. Kabalnov, E. D. Shchukin, *Advances in Colloid and Interface Science* **1992**, *38*, 69.
[28] D. V. Talapin, A. L. Rogach, M. Haase, H. Weller, *The Journal of Physical Chemistry B* **2001**, *105*, 12278.
[29] R. Borg, G. Dienes, *The Physical Chemistry of Solids* Academic Press Boston **1992**.
[30] H. Cölfen, S. Mann, *Angewandte Chemie International Edition* **2003**, *42*, 2350.
[31] B. Gilbert, H. Zhang, F. Huang, M. Finnegan, G. Waychunas, J. Banfield, *Geochemical Transactions* **2003**, *4*, 20.
[32] R. L. Penn, J. F. Banfield, *Geochem Cosmochim Acta* **1999**, *63*, 1549
[33] R. L. Penn, J. F. Banfield, *Am Mineral* **1998**, *83*, 1077
[34] G. Oskam, Z. Hu, R. L. Penn, N. Pesika, P. C. Searson, *Phys Rev E* **2002**, *66*, 11403.
[35] J. F. Banfield, S. A. Welch, H. Zhang, T. T. Ebert, R. L. Penn, *Science* **2000**, *289*, 751

[36] M. A. Watzky, R. G. Finke, *Journal of the American Chemical Society* **1997**, *119*, 10382.
[37] J. Turkevich, P. C. Stevenson, J. Hillier, *Faraday Discuss. Chem. Soc.* **1951**, *11*, 55.
[38] E. Matijevic, *Chem. Mater.* **1993**, *5*, 412.
[39] J. Overbeek, *Th. G. Adv. Colloid Interf. Sci.* **1982**, *15*, 251.
[40] J.-B. Salmon, C. Dubrocq, P. Tabeling, S. Charier, D. Alcor, L. Jullien, F. Ferrage, *Analytical Chemistry* **2005**, *77*, 3417.
[41] T. L. Sounart, P. A. Safier, J. A. Voigt, J. Hoyt, D. R. Tallant, C. M. Matzke, T. A. Michalske, *Lab on a Chip* **2007**, *7*, 908.
[42] J. B. Knight, A. Vishwanath, J. P. Brody, R. H. Austin, *Phys. Rev. Lett.* **1998**, *80*, 3863.
[43] R. Massart, V. Cabuil, *J. Chim. Phys.* **1987**, *84*, 7.
[44] N. Fauconnier, J. N. Pons, J. Roger, A. Bee, *Journal of Colloid and Interface Science* **1997**, *194*, 427.
[45] A. Bee, R. Massart, S. Neveu, *Journal of Magnetism and Magnetic Materials* **1995**, *149*, 6.
[46] S. Neveu-Prin, V. Cabuil, R. Massart, P. Escaffre, J. Dussaud, *Journal of Magnetism and Magnetic Materials* **1993**, *122*, 42.
[47] G. B. Biddlecombe, Y. K. Gun'ko, J. M. Kelly, S. C. Pillai, J. M. D. Coey, M. Venkatesan, A. P. Douvalis, *Journal of Materials Chemistry* **2001**, *11*, 2937.
[48] J. Wan, W. Cai, J. Feng, X. Meng, E. Liu, *J. Mater. Chem.* **2007**, *17*, 1188.
[49] M. Kimata, D. Nakagawa, M. Hasegawa, *Powder Technology* **2003**, *132*, 112.
[50] A. B. Chin, I. I. Yaacob, *J. Mater. Process. Technol.* **2007**, *191*, 235.
[51] G. Salazar-Alvarez, M. Muhammed, A. A. Zagorodni, *Chemical Engineering Science* **2006**, *61*, 4625.
[52] S. Basak, D. R. Chen, P. Biswas, *Chem. Eng. Sci.* **2007**, *62*, 1263.
[53] A. Bell, E. Matijevic, *The Journal of Physical Chemistry* **1974**, *78*, 2621.
[54] J. P. Jolivet, C. Froidefond, A. Pottier, C. Chaeneac, S. Cassaignon, E. Tronc, P. Euzen, *J. Mater. Chem.* **2004**, *14*, 3281.
[55] L. Vayssières, C. Chanéac, E. Tronc, J. P. Jolivet, *Journal of Colloid and Interface Science* **1998**, *205*, 205.
[56] J. P. Jolivet, P. Belleville, E. Tronc, J. Livage, *Clays Clay Miner.* **1992**, *40*, 531.
[57] J. P. Jolivet, L. Vassiere, C. Chaeneac, E. Tronc, *Mat. Res. Symp. Proc.* **1997**, *432*, 145.
[58] J. P. Jolivet, C. Chaeneac, *Tronc. Comp. Rend. Series* **2002**, *5*, 659.
[59] L. Babes, B. Denizot, G. Tanguy, J. J. Le Jeune, P. Jallet, *Journal of Colloid and Interface Science* **1999**, *212*, 474.
[60] N. Fauconnier, A. Bee, J. Roger, J. N. Pons, *Prog. Colloid Polym. Sci.* **1996**, *100*, 212.
[61] N. Fauconnier, A. Bee, J. Roger, J. N. Pons, *J. Mol. Liq.* **1999**, *83*, 233.
[62] J. Roger, J. N. Pons, R. Massart, A. Halbreich, J. C. Bacri, *Eur. Phys. J. Appl. Phys.* **1999**, *5*, 321.
[63] B. Denizot, G. Tanguy, F. Hindre, E. Rump, J. J. LeJeune, P. Jallet, *J. Colloid Interface Sci.* **1999**, *209*, 66.
[64] N. Fauconnier, A. Bée, J. Roger, J. N. Pons, *Journal of Molecular Liquids* **1999**, *83*, 233.
[65] C. Liu, P. M. Huang, *Soil Sci Soc Am J* **1999**, *63*, 65.
[66] P. R. Tremaine, J. C. LeBlanc, *Journal of Solution Chemistry* **1980**, *9*, 415.
[67] F. H. Sweeton, C. F. Baes, *J. Chem. Theromodynamic* **1970**, *2*, 479.
[68] T. Hyeon, S. S. Lee, J. Park, Y. Chung, H. B. Na, *J. Am. Chem. Soc.* **2001**, *123*, 12798.
[69] S. Sun, H. Zeng, *J. Am. Chem. Soc.* **2002**, *124*, 8204.

[70] N. R. Jana, Y. Chen, X. Peng, *Chem. Mater.* **2004**, *16*, 3931.
[71] J. Park, K. An, Y. Hwang, J.-G. Park, H.-J. Noh, J.-Y. Kim, J.-H. Park, N.-M. Hwang, T. Hyeon, *Nat. Mater.* **2004**, *3*, 891.
[72] P. Tartaj, C. J. Serna, *J. Am. Chem. Soc.* **2003**, *125*, 15754.
[73] S. Sato, T. Murakata, H. Yanagi, F. Miyasaka, S. Iwaya, *J. Mater. Sci.* **1994**, *29*, 5657.
[74] D. Jézéquel, J. Guenot, N. Jouini, F. Fieévet, *J. Mater. Res.* **1995**, *10*, 77.
[75] C. Feldmann, H.-O. Jungk, *Angewandte Chemie International Edition* **2001**, *40*, 359.
[76] V. K. Tzitzios, D. Petridis, I. Zafiropoulou, G. Hadjipanayis, D. Niarchos, *J. Magn. Magn. Mater.* **2005**, *294*, e95.
[77] G. M. Chow, L. K. Kurihara, K. M. Kemner, P. E. Schoen, W. T. Elam, A. Ervin, S. Keller, Y. D. Zhang, J. Budnick, T. Ambrose, *J. Mater. Res.* **1995**, *10*, 1546.
[78] G. Viau, F. Ravel, O. Acher, F. Fivet-Vincent, F. Fivet, *J. Appl. Phys.* **1994**, *76*, 6570.
[79] G. Viau, F. Ravel, O. Acher, F. Fivet-Vincent, F. Fivet, *J. Magn. Magn. Mater.* **1995**, *140*, 377.
[80] G. Viau, F. Fivet-Vincent, F. Fivet, *Solid State Ionics* **1996**, *84*, 259.
[81] D. Mercier, J. C. S. Lvy, G. Viau, F. Fivet-Vincent, F. Fivet, P. Toneguzzo, O. Acher, *Phys. Rev. B: Condens. Matter Mater. Phys.* **2000**, *62*, 532.
[82] C. Feldmann, *AdV. Mater.* **2001**, *13*, 1301.
[83] A. K. Giri, K. M. Chowdary, S. A. Majetich, *Mater. Phys. Mech.* **2000**, *1*, 1.
[84] W. Cai, J. Wan, *J. Colloid Interface Sci.* **2007**, *305*, 366.
[85] R. J. Joseyphus, D. Kodama, T. Matsumoto, Y. Sato, B. Jeyadevan, K. Tohji, *J. Magn. Magn. Mater.* **2007**, *310*, 2393.
[86] D. Caruntu, G. Caruntu, Y. Chen, C. J. O'Connor, G. Goloverda, V. L. Kolesnichenko, *Chemistry of Materials* **2004**, *16*, 5527.
[87] P. A. Dresco, V. S. Zaitsev, R. J. Gambino, B. Chu, *Langmuir* **1999**, *15*, 1945.
[88] S. Santra, R. Tapec, N. Theodoropoulou, J. Dobson, A. Hebard, W. Tan, *Langmuir* **2001**, *17*, 2900.
[89] F. C. Meldrum, B. R. Heywood, S. Mann, *Science* **1992**, *257*, 522.
[90] C. Sangregorio, J. K. Wieman, C. Oâ€™Connor, Z. Rosenzweig, *J. Appl. Phys.* **1999**, *85*, 5699.
[91] E. Strable, J. W. M. Bulte, B. Moskowitz, K. Vivekanandan, M. Allen, T. Douglas, *Chem. Mater.* **2001**, *13*, 2201.
[92] D. Bonacchi, A. Caneschi, D. Dorignac, A. Falqui, D. Gatteschi, D. Rovai, C. Sangregorio, R. Sessoli, *Chem. Mater.* **2004**, *16*, 2016.
[93] M. P. Pileni, N. Duxin, *Chem. Innov.* **2000**, *30*, 25.
[94] K. Inouye, R. Endo, Y. Otsuka, K. Miyashiro, K. Kaneko, T. Ishikawa, *J. Phys. Chem.* **1982**, *86*, 1465.
[95] Y. Lee, J. Lee, C. J. Bae, J. G. Park, H. J. Noh, J. H. Park, J. H. Hyeron, *Adv. Funct. Mater.* **2005**, *3*, 503.
[96] L. Frenz, A. El Harrak, M. Pauly, S. Bégin-Colin, Andrew D. Griffiths, J.-C. Baret, *Angew. Chem. Int. Ed.* **2008**, *47*, 6817.
[97] A. Abou-Hassan, O. Sandre, S. Neveu, V. Cabuil, *Angewandte Chemie International Edition* **2009**, *48*, 2342.
[98] V. P. Andreev, S. B. Koleshko, D. A. Holman, L. D. Scampavia, G. D. Christian, *Analytical Chemistry* **1999**, *71*, 2199.
[99] L. D. Scampavia, G. Blankenstein, J. Ruzicka, G. D. Christian, *Analytical Chemistry* **1995**, *67*, 2743.
[100] A. Abou-Hassan, J. F. Dufreche, O. Sandre, G. Mériguet, O. Bernard, V. Cabuil, *Lab Chip* **2009,** submitted.
[101] D. K. Kim, M. Mikhaylova, Y. Zhang, M. Muhammed, *Chemistry of Materials* **2003**, *15*, 1617.

[102] D. Margulies, G. Melman, A. Shanzer, *Nat. Mater.* **2005**, *4*, 768.
[103] N. O. Nunez, M. P. Morales, P. Tartaj, C. J. Serna, *J. Mater. Chem.* **2000**, *10*, 2561.
[104] G. J. Vroege, D. M. E. Thies-Weesie, A. V. Petukhov, B. J. Lemaire, P. Davidson, *Advanced Materials* **2006**, *18*, 2565.
[105] B. J. Lemaire, P. Davidson, J. Ferré, J. P. Jamet, D. Petermann, P. Panine, I. Dozov, J. P. Jolivet, *Europ. phys. j. E* **2004**, *13*, 291.
[106] U. Schwertmann, E. Murad, *Clays. Clay. Miner* **1983**, *31*, 277.
[107] R. L. Penn, J. F. Banfield, *Science* **1998**, *279*, 1519
[108] S. Krehula, S. Popovic, S. Music, *Mater. lett.* **2002**, *54*, 108.
[109] D. M. E. Thies-Weesie, J. P. de Hoog, M. H. Hernandez Mendiola, A. V. Petukhov, G. J. Vroege, *Chemistry of Materials* **2007**, *19*, 5538.
[110] M. Stjerndahl, M. Andersson, H. E. Hall, D. M. Pajerowski, M. W. Meisel, R. S. Duran, *Langmuir* **2008**, *24*, 3532.
[111] M. D. Alcala, C. Real, *Solid State Ionics* **2006**, *177*, 955.
[112] Y. Gushikem, S. S. Rosatto, *J. Braz. Chem. Soc.* **2001**, *12*, 695.
[113] P. Sharma, S. Brown, G. Walter, S. Santra, B. Moudgil, *Adv. Colloid Interface Sci.* **2006**, 123.
[114] Y. A. Barnakov, M. H. Yu, Z. Rosenzweig, *Langmuir* **2005**, *21*, 7524.
[115] Y. H. Deng, C. C. Wang, X. Z. Shen, W. L. Yang, L. An, H. Gao, S. K. Fu, *Chem. Eur. J.* **2005**, *11*, 6006.
[116] A. H. Lu, E. L. Salabas, F. Schueth, *Angew. Chem., Int. Ed.* **2007**, *46*, 1222.
[117] Z. Z. Xu, C. C. Wang, W. L. Yang, S. K. Fu, *J. Mater. Sci.* **2005**, *40*, 4667.
[118] P. Tartaj, T. Gonzalez-Carreno, O. Bomati-Miguel, C. J. Serna, P. Bonville, *Phys. Rev. B: Condens. Matter* **2004**, 69.
[119] N. Pamme, *Lab on a Chip* **2006**, *6*, 24.